

## Electrocaloric effects in multiferroics

Zhijun Jiang,<sup>1,2,3</sup> Bin Xu,<sup>4</sup> Sergey Prosandeev,<sup>2</sup> Yousra Nahas,<sup>2</sup> Sergei Prokhorenko,<sup>2</sup> Jorge Íñiguez,<sup>5,6</sup> and L. Bellaiche<sup>2</sup>

<sup>1</sup>MOE Key Laboratory for Nonequilibrium Synthesis and Modulation of Condensed Matter,  
School of Physics, Xi'an Jiaotong University, Xi'an 710049, China

<sup>2</sup>Physics Department and Institute for Nanoscience and Engineering,  
University of Arkansas, Fayetteville, Arkansas 72701, USA

<sup>3</sup>Key Laboratory of Computational Physical Sciences (Ministry of Education),

State Key Laboratory of Surface Physics, and Department of Physics, Fudan University, Shanghai 200433, China

<sup>4</sup>Jiangsu Key Laboratory of Thin Films, School of Physical Science and Technology, Soochow University, Suzhou 215006, China

<sup>5</sup>Materials Research and Technology Department, Luxembourg Institute of Science and Technology,  
5 Avenue des Hauts-Fourneaux, L-4362, Esch/Alzette, Luxembourg

<sup>6</sup>Physics and Materials Science Research Unit, University of Luxembourg, 41 Rue du Brill, L-4422 Belvaux, Luxembourg

An atomistic effective Hamiltonian is used to compute electrocaloric (EC) effects in rare-earth substituted BiFeO<sub>3</sub> multiferroics. A phenomenological model is then developed to interpret these computations, with this model indicating that the EC coefficient is the sum of two terms, that involve electric quantities (polarization, dielectric response), the antiferromagnetic order parameter, and the coupling between polarization and antiferromagnetic order. The first one depends on the polarization and dielectric susceptibility, has the analytical form previously demonstrated for ferroelectrics, and is thus enhanced at the ferroelectric Curie temperature. The second one explicitly involves the dielectric response, the magnetic order parameter and a specific magneto-electric coupling, and generates a peak of the EC response at the Néel temperature. These atomistic results and phenomenological model may be put in use to optimize EC coefficients.

The electrocaloric (EC) effect is a phenomenon by which a material exhibits a reversible temperature change under the application/removal of an electric field [1–5]. It is attracting attention due to its potential to be an efficient solid-state refrigeration technology (see, e.g., Refs. [6–19] and references therein).

Furthermore, multicaloric effects that are driven simultaneously by more than one type of external physical handle, such as electric and/or magnetic fields, mechanical stress and pressure [20–24], are also promising to enhance change in temperature [23, 24].

Recently, multiferroics, which are materials that possess coupled long-range-ordered electric and magnetic degrees of freedom [25–31], have also been mentioned as possible systems to enhance the EC effects by taking advantage of such coupling [12, 20, 21, 32–34]. The pioneering work of Ref. [33] started from a phenomenological Landau-type equation for which coefficients were determined from first principles to investigate how magnetoelectric coupling modifies the EC coefficient. The main result was that EC effects are significantly enhanced (by about 60%) thanks to magnetoelectric coupling in the case that the ferroelectric and magnetic critical temperatures coincide. However, one has to be careful when using a Landau-type approach because fluctuations, which can be important for responses, are not treated explicitly and may be underestimated. That is why atomistic approaches incorporating couplings between electric dipoles and spins can be useful to also study EC effects in multiferroics, as the authors of Ref. [33] indicated. More importantly, it is presently unclear how to understand EC coefficients in multiferroics. For instance, can these coefficients be considered as composed of two terms, with one corresponding to that occurring in normal ferroelectrics and the second one related to the coupling between spins and electric dipoles? If yes, what are the precise

quantities involved in the second term? Are they only magneto-electric, or rather also involve electric and/or magnetic properties? Answering such questions will help in designing systems with large EC response.

The aim of this Letter is to resolve all these issues by (1) conducting atomistic-based simulations; (2) developing a simple model that can reproduce these simulations; and (3) using such simulations and model to gain a deep microscopic insight. We demonstrate that the EC coefficient of multiferroics can be thought as having two parts, each associated with different physical quantities.

Here, we adopt the effective Hamiltonian ( $H_{\text{eff}}$ ) approach developed in Ref. [35] to study disordered Bi<sub>1-x</sub>Nd<sub>x</sub>FeO<sub>3</sub> (BNFO) alloys.  $H_{\text{eff}}$  parameters are provided in the Supplemental Material (SM) [36]. This  $H_{\text{eff}}$  successfully reproduced the temperature-*versus*-compositional phase diagram of BNFO. It predicts a  $R3c$  ground state for small Nd compositions and a  $Pnma$  phase for larger concentrations, with intermediate complex states in-between. Moreover, within the compositional range for which the  $R3c$  phase is the ground state, the ferroelectric Curie temperature  $T_C$  was numerically found to significantly decrease with the Nd composition while the  $T_N$  Néel temperature is mostly independent of concentration, which also agrees with measurements [51–53]. The total internal energy of this  $H_{\text{eff}}$  can be expressed as a sum of two main terms:

$$E_{\text{tot}} = E_{\text{BFO}}(\{\mathbf{u}_i\}, \{\eta_H\}, \{\eta_I\}, \{\boldsymbol{\omega}_i\}, \{\mathbf{m}_i\}) + E_{\text{alloy}}(\{\mathbf{u}_i\}, \{\boldsymbol{\omega}_i\}, \{\mathbf{m}_i\}, \{\eta_{\text{loc}}\}), \quad (1)$$

where  $E_{\text{BFO}}$  is the  $H_{\text{eff}}$  of pure BiFeO<sub>3</sub> [39–42] and  $E_{\text{alloy}}$  characterizes the effect of substituting Bi by Nd ions. The  $H_{\text{eff}}$  of BNFO contains four types of degrees of freedom: (i)

the local soft mode  $\{\mathbf{u}_i\}$  centered on the A site of Bi or Nd ions in the 5-atom unit cell  $i$  (which is proportional to the local electric dipole moment of that cell [43, 44]); (ii) the strain tensor gathering homogeneous  $\{\eta_H\}$  and inhomogeneous  $\{\eta_I\}$  contributions [43, 44]; (iii) the pseudovectors  $\{\omega_i\}$  that represent the oxygen octahedral tiltings [45]; and (iv) the magnetic moments  $\{\mathbf{m}_i\}$  centered on Fe ions [54].

We employ this  $H_{\text{eff}}$  within Monte Carlo (MC) simulations on  $12 \times 12 \times 12$  supercells (containing 8 640 atoms) with periodic boundary conditions and inside which Bi and Nd ions are randomly distributed over the A sublattice. 20 000 MC sweeps are used for equilibration and an additional 20 000 MC sweeps are employed to compute statistical averages at finite temperature, to obtain converged results. We also average our results over 10 random Bi/Nd distributions, to mimic well disordered BNFO solid solutions.

Regarding the linear EC coefficient,  $\alpha_\gamma$ , it is the derivative of the temperature with respect to electric field at constant entropy. It can be obtained from MC simulations by taking advantage of the cumulant formula [16, 17, 55]:

$$\alpha_\gamma = -Z^* a_{\text{lat}} T \left\{ \frac{\langle u_\gamma E_{\text{tot}} \rangle - \langle u_\gamma \rangle \langle E_{\text{tot}} \rangle}{\langle E_{\text{tot}}^2 \rangle - \langle E_{\text{tot}} \rangle^2 + \frac{21(k_B T)^2}{2N}} \right\}, \quad (2)$$

where  $Z^*$  is the Born effective charge associated with the local mode,  $a_{\text{lat}}$  represents the five-atom lattice constant,  $T$  is the temperature,  $u_\gamma$  is the  $\gamma$ -component of the supercell average of the local mode with  $\gamma = x, y, \text{ or } z$  (note that the  $x, y, \text{ and } z$  axis are chosen along the pseudocubic [100], [010] and [001] directions, respectively),  $E_{\text{tot}}$  is the total internal energy given by the  $H_{\text{eff}}$ ,  $k_B$  is the Boltzmann constant,  $N$  is the number of sites in the supercell, and  $\langle \rangle$  defines the average over the MC sweeps at a given temperature [56]. In the following, we will denote  $\alpha$  the quantity defined by  $\frac{\alpha_x + \alpha_y + \alpha_z}{\sqrt{3}}$ . Such definition corresponds to the EC response for an electric field applied along [111], which is the maximal response within a  $R3c$  state.

Figure 1 shows the EC coefficient as a function of temperature for four different Nd compositions in disordered  $\text{Bi}_{1-x}\text{Nd}_x\text{FeO}_3$ . The results of Fig. 1 are obtained by starting from 10 K adopting a  $R3c$  phase and then progressively heating up the BNFO solid solutions up to the composition-dependent Curie temperature,  $T_C$  (for all investigated temperatures displayed in Fig. 1, the disordered  $\text{Bi}_{1-x}\text{Nd}_x\text{FeO}_3$  alloys possess the  $R3c$  phase from 0 K and up to  $T_C$ ). This  $R3c$  state is characterized by a polarization lying along [111] and oxygen octahedra tilting in an antiphase fashion about this polarization's direction. These solid solutions also exhibit a G-type antiferromagnetic-to-paramagnetic transition at a Néel temperature,  $T_N$ , which is mostly independent on the composition and equal to  $\simeq 660$  K [35]. The SM [36] provides some finite-temperature properties above  $T_C$ .

Let us first focus on Fig. 1(a) that corresponds to a concentration of Nd equal to 5%. The calculated  $T_C \simeq 940$  K and  $T_N \simeq 660$  K of  $\text{Bi}_{0.95}\text{Nd}_{0.05}\text{FeO}_3$  are in rather good agreement with the measurements of  $T_C \simeq 970$  K and  $T_N \simeq 650$  K

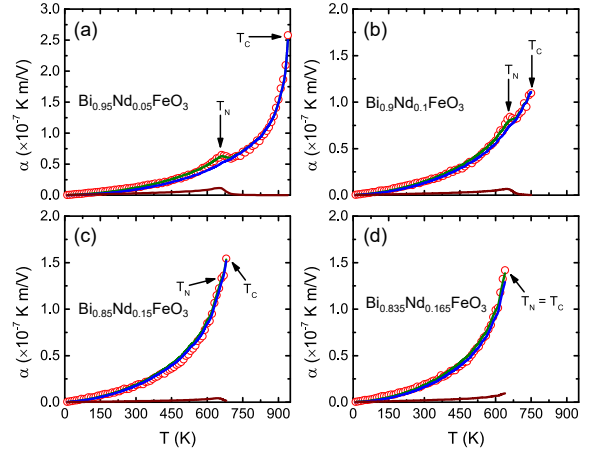


FIG. 1. Electrocaloric coefficient,  $\alpha$ , as a function of the temperature for different compositions in disordered  $\text{Bi}_{1-x}\text{Nd}_x\text{FeO}_3$  alloys: (a)  $\text{Bi}_{0.95}\text{Nd}_{0.05}\text{FeO}_3$ ; (b)  $\text{Bi}_{0.9}\text{Nd}_{0.1}\text{FeO}_3$ ; (c)  $\text{Bi}_{0.85}\text{Nd}_{0.15}\text{FeO}_3$ ; and (d)  $\text{Bi}_{0.835}\text{Nd}_{0.165}\text{FeO}_3$ . The solid green lines represent the fit of the MC results by the second line of Eq. (11), i.e.,  $\alpha = \frac{T_0 a'(T)}{C_{ph}} P_s \varepsilon_0 \chi + \frac{T_0 b'(T)}{C_{ph}} L_s \left. \frac{\partial L_s}{\partial P_s} \right|_T \varepsilon_0 \chi$ , where  $a'(T) = A_0 + A_1 T$  ( $A_0$  and  $A_1$  being fitting constants), and  $C_{ph}$  and  $b'(T)$  are also fitting parameters. The solid blue lines display the fit of the MC results by its first contribution,  $\frac{T_0 a'(T)}{C_{ph}} P_s \varepsilon_0 \chi$ . The solid brown lines correspond to the fit of the MC results by its second contribution,  $\frac{T_0 b'(T)}{C_{ph}} L_s \left. \frac{\partial L_s}{\partial P_s} \right|_T \varepsilon_0 \chi$  (see text).

[52, 53]. For any investigated temperature,  $\alpha$  basically monotonically increases when the system is heated up to the Néel temperature. It then adopts a small peak around  $T_N$ , which is found to originate from the coupling between polarization and magnetism – we verify this by running  $H_{\text{eff}}$  simulations in which the coupling between local models and magnetic moments is turned off. The EC coefficient then significantly strengthens when increasing the temperature from the end of this  $\simeq T_N$ -centered peak and up to  $T_C$ . Our predicted big value of  $\alpha$  around  $T_C$  is of the order of  $\simeq 2.6 \times 10^{-7}$  K m/V. It is thus large and close to the experimental data of  $2.5 \times 10^{-7}$  K m/V at  $T \simeq 499$  K in  $\text{PbZr}_{0.95}\text{Ti}_{0.05}\text{O}_3$  films [7] (the largest observed  $\alpha$  is equal to  $22 \times 10^{-7}$  K m/V and has been found in a  $\text{BaTiO}_3$  single crystal, see Ref. [57]) [58]. Note that  $H_{\text{eff}}$  techniques have been demonstrated in Refs. [16, 17] to accurately reproduce the EC coefficients of ferroelectrics and relaxor ferroelectrics, such as those reported in  $\text{BaTiO}_3$  [57, 59] and  $\text{Pb}(\text{Mg},\text{Nb})\text{O}_3$  [49].

Let us now concentrate on other compositions in disordered  $\text{Bi}_{1-x}\text{Nd}_x\text{FeO}_3$  alloys. Figures 1(b)-1(d) show the dependence of the EC coefficient when the Nd composition is equal to  $x = 0.10, 0.15$  and  $0.165$ , respectively. The Curie temperature  $T_C$  noticeably decreases when increasing the Nd composition, as consistent with observations and computations [35, 51–53]. Consequently, the two critical temperatures coincide, i.e.  $T_C = T_N$ , for a Nd concentration of 16.5%. Figures 1(b)-1(d) especially reveals that  $\alpha$  at the Néel temperature is enhanced when the Nd composition increases, but it becomes

more difficult to see its associated peak.

To understand the results in Fig. 1, we use a Landau free-energy potential  $F(P, L, \mathcal{E}, T)$  in which we substitute polarization  $P$  and G-type antiferromagnetic (AFM) moment  $L$  by their equilibrium values  $P_s$  and  $L_s$  found from minimization of free energy:  $\frac{\partial F}{\partial P}|_{P=P_s, \mathcal{E}, T} = 0$  and  $\frac{\partial F}{\partial L}|_{L=L_s, \mathcal{E}, T} = 0$ . The minimized free energy  $F_s(\mathcal{E}, T) = F(P_s, L_s, \mathcal{E}, T)$  has the form:

$$\begin{aligned} F_s(\mathcal{E}, T) &= \frac{1}{2}a(T)P_s^2(\mathcal{E}, T) + \frac{1}{4}\beta P_s^4(\mathcal{E}, T) \\ &\quad - \mathcal{E}P_s(\mathcal{E}, T) + \frac{1}{2}b(T)L_s^2(\mathcal{E}, T) \\ &\quad + \frac{1}{4}\kappa L_s^4(\mathcal{E}, T) + \frac{1}{2}cL_s^2(\mathcal{E}, T)P_s^2(\mathcal{E}, T), \end{aligned} \quad (3)$$

where  $\mathcal{E}$  is the electric field.

Such equation implies that the polarization implicitly depends on magnetism, because of the  $\frac{1}{2}cL_s^2(\mathcal{E}, T)P_s^2(\mathcal{E}, T)$  term. This equation is similar to the one used in Ref. [33]. The entropy described by this free energy  $F_s(\mathcal{E}, T)$ , composed of dipoles and spins, can then be obtained as

$$\begin{aligned} S_F(\mathcal{E}, T) &= - \left. \frac{dF_s}{dT} \right|_{\mathcal{E}} \\ &= - \frac{a'(T)}{2} P_s^2(\mathcal{E}, T) - \frac{b'(T)}{2} L_s^2(\mathcal{E}, T), \end{aligned} \quad (4)$$

where  $a' = da/dT$  and  $b' = db/dT$ . Note that, here we took into account that  $P_s$  and  $L_s$  are found from minimization of the free energy.

In the case of a magnetic phase transition and presence of polarization, we can consider two parts of the *total* entropy  $S(\mathcal{E}, T)$ : A first one due to electric dipoles and spins (the *active* part treated by the Landau potential above, with entropy  $S_F(\mathcal{E}, T)$ ) and a second one due to the rest of the lattice (the inert part that can be considered to be a trivial collection of harmonic phonons, with entropy  $S_{ph}(T)$ ) [60, 61]. For an adiabatic process, we have:

$$\Delta S(\mathcal{E}, T) = \Delta S_F(\mathcal{E}, T) + \Delta S_{ph}(T) = 0. \quad (5)$$

Let  $C_{ph}$  denote the heat capacity associated with the background lattice modes. Then the change of lattice entropy from an initial state  $(0, T_0)$  to the final state  $(\mathcal{E}, T)$  is given by:

$$\Delta S_{ph} = \int_{T_0}^T \frac{C_{ph}}{T} dT \cong C_{ph} \ln \left( \frac{T}{T_0} \right). \quad (6)$$

Consequently, combining Eqs. (5) and (6) leads to

$$C_{ph} \ln \left( \frac{T}{T_0} \right) = -\Delta S_F = \frac{1}{2}a'(P_s^2 - P_0^2) + \frac{1}{2}b'(L_s^2 - L_0^2). \quad (7)$$

Here  $P_s = P_s(\mathcal{E}, T)$ ,  $P_0 = P_s(0, T_0)$ ,  $L_s = L_s(\mathcal{E}, T)$ ,  $L_0 = L_s(0, T_0)$ , where  $T_0$  is the initial temperature and  $T = T_0 +$

$\Delta T$  is the final temperature ( $\Delta T$  represents the temperature change). Solving this equation with respect to  $T/T_0$  yields:

$$(T_0 + \Delta T)/T_0 = e^{[a'(P_s^2 - P_0^2) + b'(L_s^2 - L_0^2)]/2C_{ph}}. \quad (8)$$

For small  $\Delta T$ :

$$\Delta T = \frac{T_0 [a'(P_s^2 - P_0^2) + b'(L_s^2 - L_0^2)]}{2C_{ph}}. \quad (9)$$

One can then derive the following expression for  $\alpha$  [10, 16]:

$$\alpha = \left. \frac{\partial \Delta T}{\partial \mathcal{E}} \right|_S \approx \frac{T_0 a'(T)}{2C_{ph}} \left. \frac{\partial P_s^2}{\partial \mathcal{E}} \right|_T + \frac{T_0 b'(T)}{2C_{ph}} \left. \frac{\partial L_s^2}{\partial \mathcal{E}} \right|_T. \quad (10)$$

Here we assumed that, since the adiabatic temperature change is small as compared to the temperature, the constant- $S$  derivatives can be evaluated at a constant  $T = T_0$ . One can write:

$$\begin{aligned} \alpha &= \frac{T_0 a'(T)}{C_{ph}} P_s \varepsilon_0 \chi + \frac{T_0 b'(T)}{2C_{ph}} \left. \frac{\partial L_s^2}{\partial P_s} \right|_T \left. \frac{\partial P_s}{\partial \mathcal{E}} \right|_T \\ &= \frac{T_0 a'(T)}{C_{ph}} P_s \varepsilon_0 \chi + \frac{T_0 b'(T)}{C_{ph}} L_s \left. \frac{\partial L_s}{\partial P_s} \right|_T \varepsilon_0 \chi, \end{aligned} \quad (11)$$

where  $\varepsilon_0$  is the vacuum permittivity and  $\chi$  is the dielectric susceptibility. Finally, let us note that one could try to approximate  $C_{ph}$  by adding a  $k_B$  contribution for each degree of freedom belonging to the trivial – harmonic – part of the system. However, it is not obvious how to count the exact number of active and inactive variables in the framework of a Landau theory; we thus treat  $C_{ph}$  as an adjustable parameter. Note that we did not fit  $C_{ph}$  alone but rather the ratio of  $a'(T)/C_{ph}$  and  $b'(T)/C_{ph}$ .

As shown by the green lines of Fig. 1, the second line of Eq. (11) fits well the MC data, when (1) using the  $P_s$ ,  $\chi$ ,  $L_s$  and  $\frac{\partial L_s}{\partial P_s}$  [62] obtained by our Monte-Carlo simulations (these four quantities are shown in Fig. 2 for the case of a 5% Nd composition); and (2) assuming that  $C_{ph}$  and  $b'(T)$  are fitting constants, while  $a'(T) = A_0 + A_1 T$  with  $A_0$  and  $A_1$  are fitting parameters [63]. Since its validity is confirmed by Fig. 1, the second line of Eq. (11) can now be used to gain an insight [36] into the results of Fig. 1, via the decomposition of  $\alpha$  into its two terms – that are  $\frac{T_0 a'(T)}{C_{ph}} P_s \varepsilon_0 \chi$  and  $\frac{T_0 b'(T)}{C_{ph}} L_s \left. \frac{\partial L_s}{\partial P_s} \right|_T \varepsilon_0 \chi$ . The first contribution has precisely the analytical form of the EC coefficient for *non-magnetic systems*, see Refs. [16, 17]. It is shown by blue lines in Fig. 1, and is the one that contributes the most to the total  $\alpha$  for any composition. Its increases with temperature and is driven by the corresponding increase in dielectric susceptibility, however moderated by the concomitant decrease in polarization [see Figs. 2(b) and 2(a)]. This first contribution implicitly depends on magnetism because of the coupling between polarization and antiferromagnetism, as evidenced in the change of behavior of the polarization and in the occurrence of a plateau in the dielectric response near  $T_N$

(such behavior of  $\chi$  has been reported in other multiferroics [39, 64]). The second contribution of Eq. (11) is depicted in brown lines in Fig. 1, and is basically independent on the investigated composition for any temperature. As evidenced in Fig. 1, it is the one responsible for the small peak of  $\alpha$  found near the Néel temperature. This small peak becomes more difficult to be seen in the total EC coefficient (shown in green) when the Nd composition increases simply because the first contribution provides much larger values than the second contribution. Figures 2(c) and 2(d) also reveal that this small peak originates from the activation and then sharp increase of the magnitude of  $\frac{\partial L_s}{\partial P_s}$  near  $T_N$ . This derivative for temperatures far away below  $T_N$  is then basically a constant that characterizes intrinsic magnetoelectric coupling – which is related to the  $c$  constant of Eq. (3). The second term of Eq. (11) tells us that the EC coefficient of a multiferroic can be optimized even at temperatures far away  $T_N$  in systems possessing strong coupling between polarization and magnetic ordering. Ba(Sr,Ba)MnO<sub>3</sub> films may thus be a system of choice to investigate electrocaloric effects due to its strong magnetoelectric coupling [65–67].

The now-elucidated effect of  $\frac{\partial L_s}{\partial P_s}$  on  $\alpha$  near  $T_N$  can be further used to address the finite-size effects in our computations of the EC coefficient. It is known that such size effect broadens the magnetic transition when decreasing the supercell size (see the SM [36]) [47, 48], and we also checked that the magnitude of the second contribution of  $\alpha$  around  $T_N$  increases when increasing such size. It will thus be more realistic, regarding what to expect in experiments, to rather adopt a  $L_s = A|T_N - T|^\beta$  power law (see Refs. [47, 50]) near the Néel temperature, where  $A$  and  $\beta$  are coefficients. Consequently, we (1) chose to replace, around  $T_N$ , the MC data for  $L_s$  by the result given by such power law with  $\beta$  equal to 0.5 (mean-field value); (2) continue to still use the MC data for  $L_s$  for temperatures far away (below) the Néel temperature; and (3) extract  $A$  such by imposing that this power law of item (1) matches the MC data of item (2). Using the new resulting  $\frac{\partial L_s}{\partial P_s}$  along with all the previous other quantities in Eq. (11) (including the temperature behavior of the polarization) provides the data given in Fig. 3 for the second contribution but also total EC coefficient in disordered Bi<sub>0.95</sub>Nd<sub>0.05</sub>FeO<sub>3</sub> alloys. The aforementioned change of  $L_s$ 's behavior, that is a more abrupt change near  $T_N$ , leads to a narrower and stronger peak of  $\alpha$  close to the Néel temperature. The second contribution now amounts for 42% of the total EC coefficient near the magnetic transition. Such latter result is in-line with the phenomenological theory of Edström *et al.* [33] predicting that the magnetic contribution can reach approximately 60% of the electric contribution at the magnetic transition, and thus enhance the EC effect, in epitaxial multiferroic SrMnO<sub>3</sub> systems under a tensile strain of 2.63% – for which  $T_N = T_C$ . Our study explains why it is the case thanks to Eq. (11) that not only reproduces atomistic results but also and especially provides an insight into the microscopic origins of the EC effects in a multiferroic. We also used a larger supercell and such power law of  $L_s$  with different  $\beta$ , and found that our qualitative results are

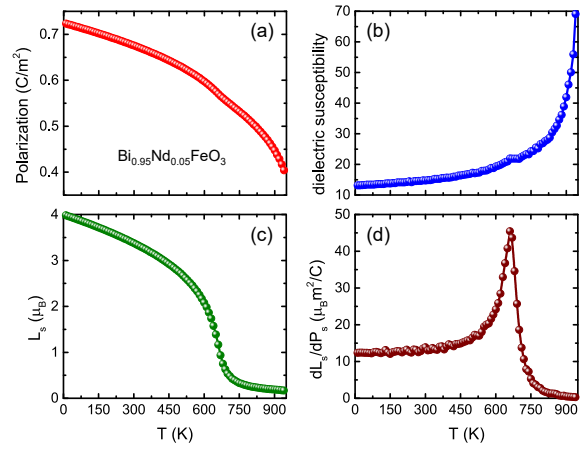


FIG. 2. Temperature dependence of some properties in disordered Bi<sub>0.95</sub>Nd<sub>0.05</sub>FeO<sub>3</sub> alloys, as obtained from our MC simulations: (a) the macroscopic polarization  $P_s$ ; (b) the average between the three diagonal elements of the dielectric susceptibility; (c) the AFM vector; and (d) the derivative  $dL_s/dP_s$ .

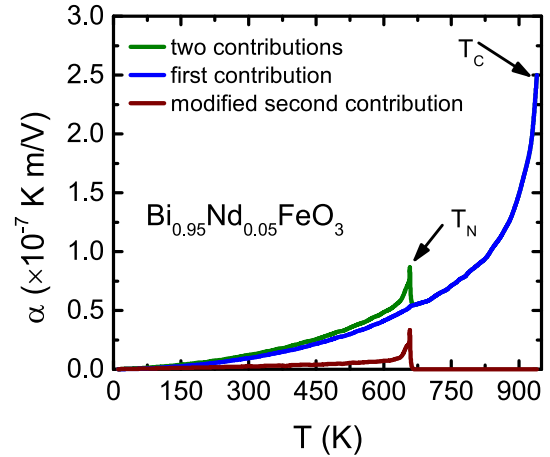


FIG. 3. Same as Fig. 1 (a) but now using a different  $\frac{\partial L_s}{\partial P_s}$  (see text) in the second line of Eq. (11).

still valid for any reasonable choice of  $\beta$  (see Fig. S3 of the SM [36]). Note that the peak of Fig. 1(a) at the Néel temperature is significantly less pronounced than in Ref. [33] for two possible reasons. The first one is that such peak depends on the size of the simulation supercell (see the SM [36]) and the second one is that the magnetoelectric coupling is weaker in BiFeO<sub>3</sub> [39] than in SrMnO<sub>3</sub> [33]. Fluctuations within the  $H_{\text{eff}}$  are also discussed in the SM [36].

In summary, an atomistic effective Hamiltonian scheme has been used to compute finite-temperature electrocaloric coefficients in the rare-earth substituted BiFeO<sub>3</sub> multiferroic. The results are then interpreted via the development of a model that reproduces these computational data. EC coefficients can be decomposed in two main terms. The first term takes its largest value at the Curie temperature and explicitly depends on the polarization and dielectric susceptibility, that are both implicit functions of magnetic ordering and strength because

of magnetoelectric couplings. The second term adopts a peak near the Néel temperature and is proportional to the antiferromagnetic vector, the polarization derivative of the antiferromagnetic vector and the dielectric susceptibility. Such findings therefore suggest an original way to induce large EC coefficients by simultaneous optimization of electric, magnetic and magnetoelectric properties at a selected temperature below the Néel temperature: (1) the dielectric susceptibility should be large; (2) the antiferromagnetic vector should be strong; and (3) the magnetoelectric coupling  $\frac{\partial L_s}{\partial P_s}$  should be large [68]. Our results and phenomenology should be valid for all magnetoelectric multiferroics, at the exception of those for which a magnetic Dzyaloshinskii-Moriya interaction involving the polarization (e.g., the spin-current model) is important. We hope that the present article deepens the fields of multiferroics and important subtle cross-coupling properties such as electrocaloric effects.

This work is supported by the National Natural Science Foundation of China (Grants No. 11804138 and No. 11825403), Shandong Provincial Natural Science Foundation (Grant No. ZR2019QA008), China Postdoctoral Science Foundation (Grants No. 2020T130120 and No. 2018M641905), “Young Talent Support Plan” of Xi’an Jiaotong University, Postdoctoral International Exchange Program of Academic Exchange Project, and Shanghai Postdoctoral Excellence Program. B. X. acknowledges financial support from National Natural Science Foundation of China (Grant No. 12074277), the startup fund from Soochow University and support from Priority Academic Program Development (PAPD) of Jiangsu Higher Education Institutions. S. Prosdandeev is supported by ONR Grant N00014-17-1-2818. Y. N., S. Prokhorenko and L. B. thank the DARPA Grants No. HR0011727183-D18AP00010 (TEE programme) and No. HR0011-15-2-0038 (MATRIX program). J. Í. acknowledges funding from the Luxembourg National Research Fund through the CORE program (Grant No. FNR/C18/MS/12705883 REFOX, J. Í.).

---

[1] M. E. Lines and A. M. Glass, *Principles and Applications of Ferroelectrics and Related Materials* (Oxford University Press, New York, 1977).  
 [2] J. F. Scott, *Science* **315**, 954 (2007).  
 [3] J. F. Scott, *Annu. Rev. Mater. Sci.* **41**, 229 (2011).  
 [4] T. Correia and Q. Zhang, *Electrocaloric Materials* (Springer, Berlin, 2014).  
 [5] Z. Kutnjak, B. Rožič, and R. Pirc, *Electrocaloric Effect: Theory, Measurements, and Applications* (Wiley Encyclopedia of Electrical and Electronics Engineering, 2015).  
 [6] K. Uchino, *Ferroelectric Devices* (Marcel Dekker, New York, 2000).  
 [7] A. S. Mischenko, Q. Zhang, J. F. Scott, R. W. Whatmore, and N. D. Mathur, *Science* **311**, 1270 (2006).  
 [8] S. Prosdandeev, I. Ponomareva, and L. Bellaiche, *Phys. Rev. B* **78**, 052103 (2008).  
 [9] I. Ponomareva and S. Lisenkov, *Phys. Rev. Lett.* **108**, 167604

(2012).  
 [10] M. C. Rose and R. E. Cohen, *Phys. Rev. Lett.* **109**, 187604 (2012).  
 [11] E. Defay, S. Crossley, S. KarNarayan, X. Moya, and N. D. Mathur, *Adv. Mater.* **25**, 3337 (2013).  
 [12] X. Moya, S. K.-Narayan, and N. D. Mathur, *Nat. Mater.* **13**, 439 (2014).  
 [13] W. Geng, Y. Liu, X. Meng, L. Bellaiche, J. F. Scott, B. Dkhil, and A. Jiang, *Adv. Mater.* **27**, 3165 (2015).  
 [14] M. Marathe, A. Grünebohm, T. Nishimatsu, P. Entel, and C. Ederer, *Phys. Rev. B* **93**, 054110 (2016).  
 [15] G. G. Guzmán-Verri and P. B. Littlewood, *APL Mater.* **4**, 064106 (2016).  
 [16] Z. Jiang, S. Prokhorenko, S. Prosdandeev, Y. Nahas, D. Wang, J. Íñiguez, E. Defay, and L. Bellaiche, *Phys. Rev. B* **96**, 014114 (2017).  
 [17] Z. Jiang, Y. Nahas, S. Prokhorenko, S. Prosdandeev, D. Wang, J. Íñiguez, and L. Bellaiche, *Phys. Rev. B* **97**, 104110 (2018).  
 [18] B. Nair, T. Usui, S. Crossley, S. Kurdi, G. G. Guzmán-Verri, X. Moya, S. Hirose, and N. D. Mathur, *Nature (London)* **575**, 468 (2019).  
 [19] J. Shi, D. Han, Z. Li, L. Yang, S.-G. Lu, Z. Zhong, J. Chen, Q. M. Zhang, and X. Qian, *Joule* **3**, 1200 (2019).  
 [20] M. M. Vopson, *Solid State Commun.* **152**, 2067 (2012); *J. Phys. D: Appl. Phys.* **46**, 345304 (2013).  
 [21] E. Stern-Taulats, T. Castán, L. Mañosa, A. Planes, N. D. Mathur, and X. Moya, *MRS Bull.* **43**, 295 (2018).  
 [22] Y. Liu, G. Zhang, Q. Li, L. Bellaiche, J. F. Scott, B. Dkhil, and Q. Wang, *Phys. Rev. B* **94**, 214113 (2016).  
 [23] I. Takeuchi and K. Sandeman, *Phys. Today* **68**, 48 (2015).  
 [24] H. Khassaf, T. Patel, and S. P. Alpay, *J. Appl. Phys.* **121**, 144102 (2017).  
 [25] G. Catalan and J. F. Scott, *Adv. Mater.* **21**, 2463 (2009).  
 [26] T. Zhao, A. Scholl, F. Zavaliche, K. Lee, M. Barry, A. Doran, M. P. Cruz, Y. H. Chu, C. Ederer, N. A. Spaldin, R. R. Das, D. M. Kim, S. H. Baek, C. B. Eom, and R. Ramesh, *Nat. Mater.* **5**, 823 (2006).  
 [27] D. Lebeugle, D. Colson, A. Forget, M. Viret, A. M. Bataille, and A. Gukasov, *Phys. Rev. Lett.* **100**, 227602 (2008).  
 [28] R. J. Zeches *et al.*, *Science* **326**, 977 (2009).  
 [29] N. A. Spaldin, S.-W. Cheong, and R. Ramesh, *Phys. Today* **63**, 38 (2010).  
 [30] B. Xu, J. Íñiguez, and L. Bellaiche, *Nat. Commun.* **8**, 15682 (2017).  
 [31] N. A. Spaldin and R. Ramesh, *Nat. Mater.* **18**, 203 (2019).  
 [32] C. Cazorla and J. Íñiguez, *Phys. Rev. B* **98**, 174105 (2018).  
 [33] A. Edström and C. Ederer, *Phys. Rev. Lett.* **124**, 167201 (2020).  
 [34] Y. Q. Zhao and H. X. Cao, *J. Mater. Sci.* **55**, 5705 (2020).  
 [35] B. Xu, D. Wang, J. Íñiguez, and L. Bellaiche, *Adv. Funct. Mater.* **25**, 552 (2015).  
 [36] See Supplemental Material at [URL will be inserted by publisher] for more details about (i) the effective Hamiltonian method and parameters; (ii) a wide range of finite-temperature properties in disordered  $\text{Bi}_{0.95}\text{Nd}_{0.05}\text{FeO}_3$  solid solutions; (iii) finite size effects on the electrocaloric (EC) coefficient in disordered  $\text{Bi}_{0.95}\text{Nd}_{0.05}\text{FeO}_3$  solid solutions; (iv) fluctuations in the effective Hamiltonian; (v) power law with different  $\beta$ ; (vi) deep new insights from the phenomenological model; and (vii) another derivation to yield our phenomenological model, which includes Refs. [37-50].  
 [37] B. Xu, D. Wang, H. J. Zhao, J. Íñiguez, X. M. Chen, and L. Bellaiche, *Adv. Funct. Mater.* **25**, 3626 (2015).  
 [38] K. Patel, S. Prosdandeev, B. Xu, and L. Bellaiche, *Phys. Rev. B* **100**, 214107 (2019).

- [39] I. A. Kornev, S. Lisenkov, R. Haumont, B. Dkhil, and L. Bellaiche, Phys. Rev. Lett. **99**, 227602 (2007).
- [40] S. Lisenkov, I. A. Kornev, and L. Bellaiche, Phys. Rev. B **79**, 012101 (2009).
- [41] D. Albrecht, S. Lisenkov, W. Ren, D. Rahmedov, I. A. Kornev, and L. Bellaiche, Phys. Rev. B **81**, 140401(R) (2010).
- [42] S. Prosandeev, D. Wang, W. Ren, J. Íñiguez, and L. Bellaiche, Adv. Funct. Mater. **23**, 234 (2013).
- [43] W. Zhong, D. Vanderbilt, and K. Rabe, Phys. Rev. Lett. **73**, 1816 (1994).
- [44] W. Zhong, D. Vanderbilt, and K. Rabe, Phys. Rev. B **52**, 6301 (1995).
- [45] I. A. Kornev, L. Bellaiche, P. E. Janolin, B. Dkhil, and E. Suard, Phys. Rev. Lett. **97**, 157601 (2006).
- [46] D. Rahmedov, D. Wang, J. Íñiguez, and L. Bellaiche, Phys. Rev. Lett. **109**, 037207 (2012).
- [47] M. Pärnaste, M. van Kampen, R. Brucas, and B. Hjörvarsson, Phys. Rev. B **71**, 104426 (2005).
- [48] J. H. Morkkath, Phys. Chem. Chem. Phys. **22**, 6275 (2020).
- [49] B. Rožič, M. Kosec, H. Uršič, J. Holc, B. Malič, Q. M. Zhang, R. Blinc, R. Pirc, and Z. Kutnjak, J. Appl. Phys. **110**, 064118 (2011).
- [50] N. W. Ashcroft and N. D. Mermin, *Solid State Physics* (Saunders College, Philadelphia, 1976).
- [51] S. Karimi, I. M. Reaney, Y. Han, J. Pokorny, and I. Sterianou, J. Mater. Sci. **44**, 5102 (2009).
- [52] I. Levin, S. Karimi, V. Provenzano, C. L. Dennis, H. Wu, T. P. Comyn, T. J. Stevenson, R. I. Smith, and I. M. Reaney, Phys. Rev. B **81**, 020103(R) (2010).
- [53] I. Levin, M. G. Tucker, H. Wu, V. Provenzano, C. L. Dennis, S. Karimi, T. Comyn, T. J. Stevenson, R. I. Smith, and I. M. Reaney, Chem. Mater. **23**, 2166 (2011).
- [54] Note that the local quantity  $\eta_{oc}(i)$  is centered on the Fe-site  $i$  and is defined as  $\eta_{oc}(i) = \frac{\delta R_{ionic}}{8} \sum_j \sigma_j$ , where  $\sigma_j$  characterizes the atomic distribution of Bi or Nd ion at the A site  $j$  and the sum over  $j$  runs over the eight A nearest neighbors of the Fe-site  $i$ .  $\delta R_{ionic}$  describes the relative difference of ionic radius between the Nd and Bi ions within the A sublattice.
- [55] S. Bin-Omran, I. A. Kornev, and L. Bellaiche, Phys. Rev. B **93**, 014104 (2016).
- [56] Note that the denominator in this expression essentially corresponds to the calculated specific heat, which has several parts. The non-trivial one is associated from the potential energy of the subsystem described by our effective Hamiltonian (local dipoles,  $O_6$  rotations, inhomogeneous strains and spins), and is given by the width of the energy distribution as obtained from our Monte Carlo simulations. The second, trivial part is associated to the kinetic contribution of all the lattice degrees of freedom in our material (15 per cell), as well as the contribution associated to the potential energy of the variables not included in our effective Hamiltonian (6 per cell); hence the term proportional to  $21k_B T/2$ . Note also that Eq. (2) is not suitable to describe situations in which the electric field induces a phase transition; hence, we restrict its application to relatively small electric fields.
- [57] X. Moya, E. Stern-Taulats, S. Crossley, D. González-Alonso, S. Kar-Narayan, A. Planes, L. Mañosa, and N. D. Mathur, Adv. Mater. **25**, 1360 (2013).
- [58] The possible electronic contribution to the EC effect is not included here since this  $H_{eff}$  does not incorporate electrons as degrees of freedom. This is probably a small effect since the major part of the polarization comes from ionic displacements.
- [59] A. Karchevskii, Sov. Phys. Solid State **3**, 2249 (1962).
- [60] R. Pirc, Z. Kutnjak, R. Blinc, and Q. M. Zhang, J. Appl. Phys. **110**, 074113 (2011).
- [61] R. Pirc, B. Rožič, J. Koruza, B. Malič, and Z. Kutnjak, EPL **107**, 17002 (2014).
- [62] For each temperature, the calculations provide  $L_s$  and  $P_s$ , which allows to plot  $L_s$  versus  $P_s$  and then to obtain the derivative of  $L_s$  with respect to  $P_s$  for any considered temperature.  $\frac{dL_s}{dP_s}$  as a function of temperature is thus obtained.
- [63] Note that the linear temperature dependence of  $a'(T)$  is needed for describing results far away from the Curie temperature, probably also because the oxygen octahedral tiltings are implicitly included in our model within some parameters of Eq. (11).
- [64] D. G. Tomuta, S. Ramakrishnan, G. J. Nieuwenhuys, and J. A. Mydosh, J. Phys.: Condens. Matter **13**, 4543 (2001).
- [65] T. Bayaraa, Y. Yang, H. J. Zhao, J. Íñiguez, and L. Bellaiche, Phys. Rev. Mater. **2**, 084404 (2018).
- [66] H. Sakai, J. Fujioka, T. Fukuda, D. Okuyama, D. Hashizume, F. Kagawa, H. Nakao, Y. Murakami, T. Arima, A. Q. R. Baron, Y. Taguchi, and Y. Tokura, Phys. Rev. Lett. **107**, 137601 (2011).
- [67] L. Maurel, N. Marcano, E. Langenberg, R. Guzmán, T. Prokscha, C. Magén, J. A. Pardo, and P. A. Algarabel, APL Mater. **7**, 041117 (2019).
- [68] In case of a ferromagnetic multiferroic, Eq. (11) needs to be altered by simply replacing the antiferromagnetic vector by the magnetization,  $M$ . All the conclusions indicated above thus still hold but when considering the magnetic Curie temperature rather than the Néel one and when involving  $\frac{\partial M}{\partial P_s}$  rather than  $\frac{\partial L_s}{\partial P_s}$ .